Size Tunable Au@Ag Core-Shell Nanoparticles: Synthesis and SERS Properties

Akshaya K. Samal, Lakshminarayana Polavarapu, Sergio Rodal-Cedeira, Luis M. Liz-Marzán, Jorge Pérez-Juste, and Isabel Pastoriza-Santos

corresponding author: pastoriza@uvigo.es

Size Tunable Au@Ag Core-Shell Nanoparticles: Synthesis and SERS Properties

Akshaya K. Samal,[†] Lakshminarayana Polavarapu, [‡] Sergio Rodal-Cedeira, [†] Luis M. Liz-Marzán,[†‡§] Jorge Pérez-Juste, [†] and Isabel Pastoriza-Santos[†]*

[†]*Departamento de Química Física, Universidade de Vigo, 36310, Spain*

[‡]*BioNanoPlasmonics Laboratory, CIC biomaGUNE, Paseo de Miramón 182, 20009 Donostia - San Sebastián, Spain*

[§]*Ikerbasque, Basque Foundation for Science, 48011 Bilbao, Spain*

ABSTRACT: We describe a simple and efficient methodology for the aqueous synthesis of stable, uniform and size tunable Au@Ag core-shell nanoparticles (NPs) which are stabilized by citrate ions. The synthetic route is based on the stepwise Ag reduction on preformed Au NPs. The final size of the core-shell NPs and therefore their optical properties can be modulated at least from 30 to 110 nm by either tuning the Ag shell thickness or changing the size of the Au core. The optical properties of the Au@Ag core-shell NPs resemble those of pure Ag NPs of similar sizes, which was confirmed by means of Mie extinction calculations. We additionally evaluated the SERS enhancing properties of Au@Ag core-shell NP colloids with three different laser lines (532, 633, and 785 nm). Importantly, such core-shell NPs also exhibit higher SERS efficiency than Ag NPs of similar size at near-infrared excitation. The results obtained here serve as a basis to select Au@Ag core-shell NPs of specific size and composition with maximum SERS efficiency at their respective excitation wavelengths for SERS-based analytical and bio-imaging applications.

INTRODUCTION

The size and shape dependent optical properties of gold and silver NPs render them suitable candidates for applications in diverse fields such as (bio)sensing, biomedicine, imaging and nanophotonics.[1-4] Various synthetic routes have been developed that allow us to control NPs size, shape and surface chemistry, which are crucial parameters for both fundamental studies and applications. Although gold is often more suited for biomedical applications due to high biocompatibility, chemical stability and easy surface modification,[5] silver is more attractive for optoelectronics, photovoltaics and sensing, because of a higher plasmonic efficiency[6] and superior electromagnetic enhancement in the visible.[7-9] Thus, Ag nanocrystals exhibit stronger Raman[8] and fluorescence enhancements,[10] larger solar energy conversion efficiencies and higher refractive index sensitivities.[11]

Ag nanocrystals of different shapes (spheres,[12] wires,[13] prisms,[14] cubes,[15] etc.) have been successfully synthesized, but suitable size control is only possible in few cases.[16-19] In the case of spherical Ag particles, size control and monodispersity are still challenging problems. Evanoff et al.[19] succeeded to synthesize uniform Ag nanospheres in a wide size range from 10 to 200 nm, on the basis of the reduction of a supersaturated Ag_2O solution at 70 ºC by pressurized hydrogen gas. Apart from this cumbersome method, the control over the size and uniformity of Ag nanospheres in a wide size range has remained rather limited.[12,20] For example, the conventional citrate reduction of $AgNO_3$, commonly used for the preparation of Ag nanocrystals, yields polydisperse Ag NPs.[21,22] These obstacles limit the utility of plasmonic Ag nanospheres as building blocks to fabricate active plasmonic devices, as well as in various plasmon based applications.

On the other hand, unlike Ag spheres, uniform Au spherical NPs of different sizes in the 15-200 nm range, can be prepared by conventional citrate reduction method,[23,24] by strategies using citrate as stabilizing agent[25,26] or by various other methods involving surfactants and polymers.[27,28] Therefore, we propose that an alternative to the synthesis of pure Ag spheres might be the use of preformed Au spheres as templates, especially considering that in bimetallic core-shell NPs the outermost layer dominates the interaction with light (electromagnetic fields decay exponentially inside metals).[29] Indeed, in the case of Au nanorods it has been demonstrated that the growth of thin Ag shells gives rise to particles with similar optical properties to those displayed by pure Ag NPs.[30] Several research groups also attempted to prepare spherical Au@Ag core-shell NPs depositing Ag on Au cores.[28,30-34] Although some success has been achieved in the synthesis of Au@Ag core-shell spherical NPs, control over a wide size range, uniformity and composition of the NPs still has certain limitations. Furthermore, most of the synthetic strategies make use of surfactants (e.g. cetyltrimethylammonium bromide, CTAB) and polymers (e.g. polyvinylpyrrolidone, PVP) as capping agents, which restrict the application of these materials in SERS or biosensing since they prevent reporter molecule adsorption on the nanoparticle surface or interfere with the identification of the compounds of interest.

Surfactant free Au@Ag core-shell NPs with Ag-like optical properties are expected to be ideal candidates for SERS studies,[8,34-35] but their size correlated and excitation wavelength dependent SERS studies have not been reported in detail due to the limitations of their size controlled synthesis, unlike gold NPs. Working towards this direction, we report a simple methodology for the preparation of Au@Ag core-shell NPs in water, which are stabilized by citrate. The method is based on the gradual coating of citrate stabilized Au nanoparticles with Ag shells, obtaining particles with Ag-like optical properties. The size of the final core-shell NPs

was varied by either changing Au core size or Ag shell thickness. Citrate-stabilized Au@Ag core-shell NPs were prepared in sizes ranging from 30 to 110 nm and their UV-visible absorbance spectra were compared with calculated extinction spectra for both Au@Ag core-shell and pure Ag NPs of the same size. Additionally, the SERS enhancing properties of Au@Ag core-shell NPs of three different sizes were studied at three different excitation laser lines (532, 633 and 785 nm). The SERS efficiency of such Au@Ag core-shell NPs was compared with that of Ag NPs of similar average size obtained by conventional citrate reduction method at three different excitation lasers.

EXPERIMENTAL SECTION

Chemicals: Tetrachloroauric acid ($HAuCl_4 \cdot 3H_2O$), L-ascorbic acid +99% (AA), trisodium citrate dihydrate, silver nitrate +99% ($AgNO_3$), and sodium hydroxide pellets +97% (NaOH) were purchased from Aldrich and used as received. 1-naphthalenethiol (1-NAT) was obtained from Acros Organics. Milli-Q water with a resistivity higher than 18.2 MΩ cm was used throughout the experiments.

Synthesis of Au NPs: ~15 nm of citrate-stabilized Au NPs were synthesized by Turkevich method.[35] 5 mL of trisodium citrate (0.5 %) was added to 95 mL boiling aqueous solution containing $HAuCl_4$ (0.5 mM). The solution was kept boiling for 15 min and then cooled down to room temperature. Citrate-stabilized Au NPs of ~32 and 55 nm in diameter were prepared by kinetically controlled seeded growth method reported by Bastús *et al*.[23] Briefly, 150 mL of 2.2 mM trisodium citrate in Milli-Q water was heated to boiling under vigorous stirring. After 15 min, 1 mL of 25 mM $HAuCl_4$ was injected into the boiling reaction mixture and after 10 min the reaction was cooled down to 90 °C. Subsequently, 1 mL of 25 mM $HAuCl_4$ aqueous solution

was injected into the reaction mixture and after 30 min 1 mL of the same solution was injected again. After 30 more min, 55 mL of the sample was extracted and 53 mL of water and 2.2 mL of 60 mM sodium citrate were added. The final solution was then used as a seed solution and the process was repeated (but with just two injections of $HAuCl_4$ aqueous solution) again for 3 and 5 times to obtain 32 and 55 nm Au NPs, respectively.

Synthesis of Au@Ag core-shell NPs.

15 nm Au seeds: For the first cycle, 60 μL AA (100 mM), 15 μL $AgNO_3$ (100 mM) and 75 μL NaOH (100 mM) were added to a beaker containing 10 mL of as prepared Au NPs (~15 nm) at room temperature. The pH of the mixture was around 8.5. The reaction was continued for 30 minutes under slow stirring before performing a new addition of 60 μL AA (100 mM), 15 μL $AgNO_3$ (100 mM) and 75 μL NaOH (100 mM). After a selected number of additions the resulting particles were centrifuged at 1800 rpm for 20 min and redispersed in 10 mL of water.

32 and 55 nm Au seeds: When Au colloids of ~32 and 55 nm were used as seeds the concentrations of reactants ($AgNO_3$, AA, NaOH) in each addition were increased 2- and 3-fold, respectively. The rest of the process was identical to that described for 15 nm Au seeds. The gradual increase of Ag shell thickness was monitored by UV-visible spectroscopy and transmission electron microscopy (TEM). The samples are centrifuged at 1800 rpm to remove excess reagents and the residue was redispersed in deionized water for SERS studies.

Synthesis of citrate reduced Ag NPs: Ag NPs were synthesized by the citrate reduction method.[21] $AgNO_3$ (4.5 mg) was dissolved in 100 mL of deionised water and heated to boiling. Then, 2 mL of 1% sodium citrate solution was added to the boiling solution and boiling was maintained for 1 h to obtain Ag NPs of ~70 nm diameter.

Characterization: UV-visible-NIR spectra were recorded using an Agilent 8453 spectrophotometer in the range of 190-1100 nm, using 10 mm path length quartz cuvettes. TEM images were obtained with a JEOL JEM 1010 microscope operating at an acceleration voltage of 100 kV. Size distributions were determined from TEM images using more than 100 NPs for each sample. Z-Potential was determined through electrophoretic mobility measurements using a Zetasizer Nano S (Malvern Instruments, Malvern UK).

Simulation of extinction spectra: Numerical simulations of extinction spectra of Au@Ag core-shell NPs and pure Ag NPs were carried out using the commercial program MQMie 3.1. Near field enhancement maps were calculated using the boundary element method (BEM).[37,38] The experimental system was simulated using a concentric spheres (core-shell) model. The diameters of the NPs core and shell were based on the dimensions determined from TEM. The frequency-dependent dielectric functions for Au and Ag were taken from ref. 38 and we used an index of refraction 1.333 for water.

SERS studies: Samples for SERS measurements in solution were prepared by adding 10 μL of 10^{-4} M 1-NAT to 1 mL of 0.05 nM (particle number concentration) Ag or Au@Ag core-shell NPs. The samples were shaken for 3h using a mechanical shaker to reach thermodynamic equilibrium and then average SERS signals were directly recorded from these suspensions using a Renishaw Invia system, equipped with Peltier charge-coupled device (CCD) detectors and a Leica confocal microscope. SERS signals from the samples were collected upon excititation with three different laser lines (532, 633, and 785 nm).

RESULTS AND DISCUSSION

The synthetic strategy toward Au@Ag core-shell NPs with size control is based on the gradual reduction of Ag^+ ions, through stepwise addition of $AgNO_3$ to a solution containing preformed citrate-stabilized Au NPs and a mild reducing agent, AA. Since AA is unable of reducing Ag^+ at low pH even in the presence of Au seeds, it was critical to adjust the pH to 8.5 (regulated by NaOH, see experimental section) after each $AgNO_3$ addition.[33] The use of a mild reducing agent, as well as the gradual addition of the Ag precursor ensured the reduction of Ag^+ onto the Au cores while inhibiting the formation of free Ag nuclei.[40] The final particle size could be modulated through either tuning the size of the Au NP cores or the thickness of the Ag shells (number of $AgNO_3$ additions). It is important to note that, apart from the citrate present on the initial Au cores, no additional stabilizer was required upon silver growth.

Citrate-stabilized Au NPs of different sizes (15.4 ± 1.3, 32.4 ± 3.4 and 54.5 ± 4.9 nm, see Figure S1 in supporting information, SI) were prepared by a kinetically controlled seeded growth method,[23] and subsequently used as seeds for silver growth. As shown in the TEM images (Figure 1), the gradual growth of silver on the preformed Au seeds gave rise to homogeneous coatings, resulting in Au@Ag core-shell NPs with quasi-spherical morphology. The different electron density of Au and Ag atoms provided sufficient contrast to distinguish the Au core and the Ag shell in the case of small cores or thin shells (Figure 1 and Figure S2, SI). TEM analysis not only revealed that after each addition step the Ag shells became thicker but also that no Ag nuclei were formed. However, we noticed that for 15 nm Au cores the core-shell NPs started deviating from the spherical shape as the shell thickness reached the diameter of the core (10

additions, **Figure 1C**). The dimensions listed in **Table 1** show a good

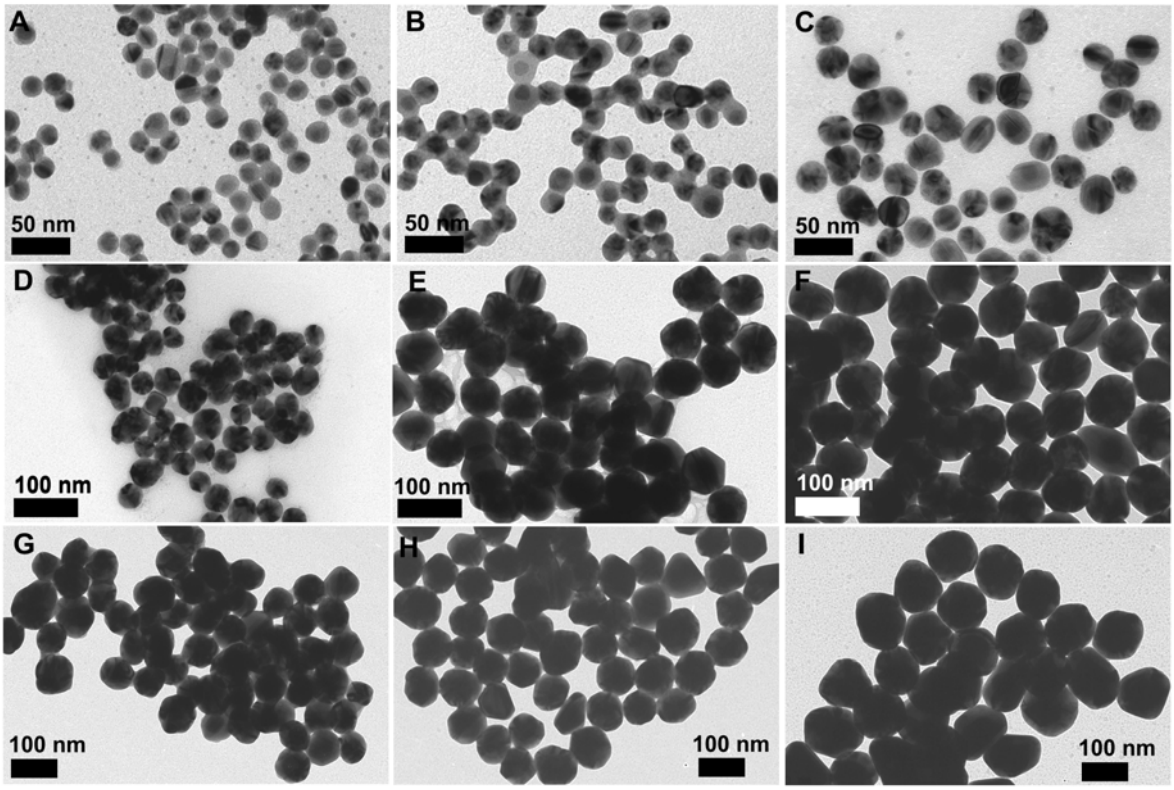

Figure 1. Representative TEM images of Au@Ag core-shell NPs obtained from citrate-stabilized Au NPs of different sizes (A-C. 15 nm; D-F. 32 nm; G-I. 55 nm) after 3 (A, D, G), 5 (B, E, H) and 10 (C, F, I) $AgNO_3$ additions.

agreement (within experimental error) between the diameter of Au@Ag NPs measured from TEM analysis and the calculated values considering that all Ag^+ ions are reduced on the Au seeds. In the same table it can be seen that the standard deviations obtained from TEM for the Au@Ag NPs formed after 3, 5 and 10 additions, remained below 10%, in agreement with the value for the corresponding Au seeds (see Table 1). In summary, by varying the Au core size and modulating the Ag shell thickness, uniform Au@Ag NPs were obtained with sizes ranging from 30 to 110 nm in diameter. In principle, there is no obvious upper limit for the particle size, since

the number of additions can be increased and larger Au seeds can be used. It should be mentioned that, non-uniform coatings, as well as nucleation of Ag NPs, were obtained when higher $AgNO_3$ concentrations were used in each reduction step (see Figure S3, SI).

Table 1. Details of the sizes of Au@Ag core-shell NPs obtained after 3, 5 and 10 $AgNO_3$ additions. The calculated sizes result from the formula provided in ref. 41 and considering that all added Ag^+ ions were reduced on the seeds.

Au seeds size/nm	Measured(calculated*) Au@Ag NP average size/nm		
	3rd addition	5th addition	10th addition
14.6 ± 1.1	21.4 ± 1.5 **(19.7),** 7%	24.3 ± 2.2 **(22.4)**, 9%	32.3 ± 2.9 **(26.8)**, 11%
32.5 ± 3.8	45.3± 5.2 **(48.0),** 11%	61.5 ± 5.4 **(58.6)**, 9%	77.1 ± 6.9 **(71.8)**, 9%
54.6 ± 5.8	79.5 ± 7.4 **(78.3),** 9%	89.0± 8.7 **(89.1)**, 10%	110±11.3 **(110.3)**, 10%

As shown in Figure 2A-C, the growth of silver shells onto preformed Au NPs led to color changes from different tones of red to orange and brown. Since the Au@Ag core-shell NPs are rather monodisperse in both size and shape, their optical properties can be safely analyzed through their UV-vis spectra (Figure 2 and Figure S4, SI). In all cases, Ag coating originated an absorption minimum in the spectrum at ca. 320 nm.[6] This spectral feature is due to Ag interband transitions in this spectral region, and is inherent to the Ag dielectric properties and thus independent of particle shape and size.[6] Additionally, the LSPR band intensity increased as more Ag was reduced, along with a significant blue-shift. Both features can be explained by the increase in particle volume and the dielectric properties of silver. A new band was also seen to gradually appear around 400 nm, which eventually merged with the band at higher wavelength

for samples with 15 and 32 nm Au cores but not for the 55 nm core sample. For Au@Ag core-shell particles larger than 70 nm, the extinction spectra also revealed a quadrupolar LSPR mode around 400 nm (see Figure 2E-F). By comparing the experimental spectra with Mie extinction calculations, a general agreement is found, especially for 15 and 32 nm cores, as shown in Figure 2. The differences between calculated and experimental spectra are likely to arise from some polydispersity in both the cores and the shells, as well as from deviations from the (concentric) spherical shape. The contribution of the Ag shell on the optical response of the Au@Ag core-shell NPs was elucidated by calculating the extinction spectra of pure Ag NPs of the same size as the Au@Ag core-shell NPs (Figure S5, SI). Regardless of the core size, gradual screening of the Au surface plasmons by those of the Ag shell is observed as more Ag is deposited. Indeed, a complete screening of the Au surface plasmons was found after 10 $AgNO_3$ additions for 15 and 32 nm Au seeds (Figure S5, SI), i.e. the optical properties of the resulting Au@Ag core-shell NPs are very similar to those expected for pure Ag nanospheres. Therefore, this seeded growth strategy allows us to fabricate NPs with Ag-like optical properties, in water and stabilized by citrate ions, which are very useful for plasmonic applications such as metal enhanced fluorescence and SERS and for a broad range of excitation wavelengths due to their size tunable extinction properties (especially in the visible excitation region).

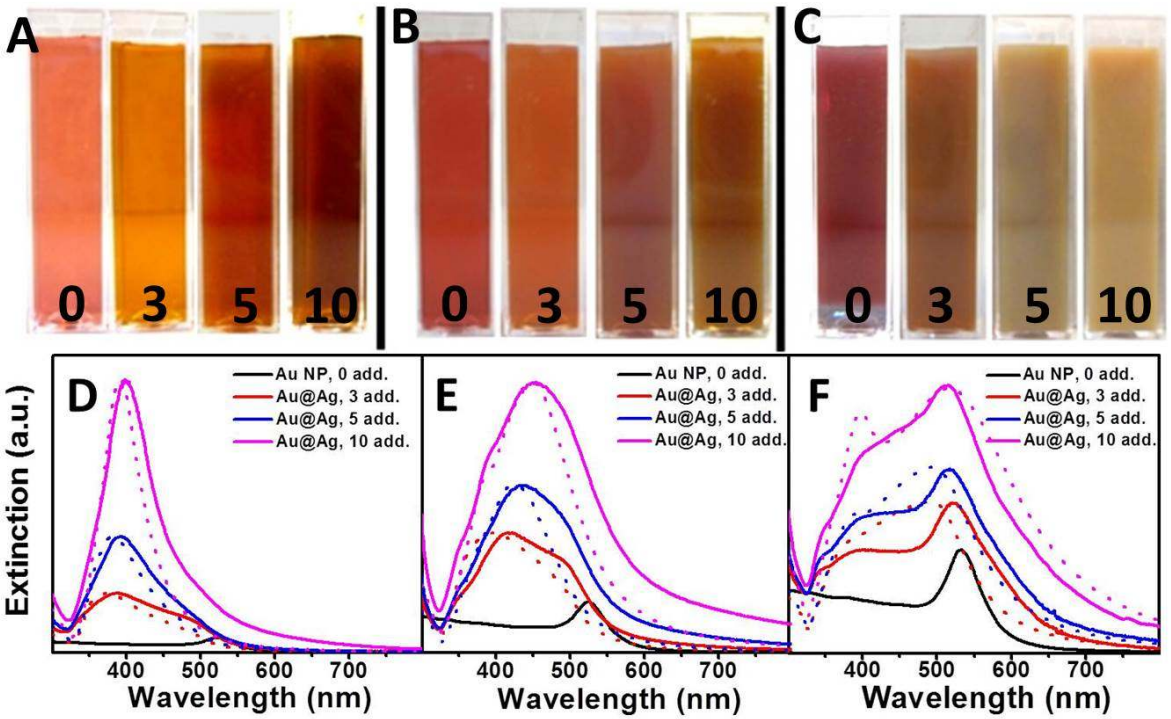

Figure 2. A-C) Color changes derived from Ag coating of 15 nm (A), ~32 nm (B) and ~55 nm (C) Au colloids (No. of Ag^+ additions are indicated in the labels). D-E) Experimental (solid lines) and calculated (dotted lines) extinction spectra of Au (black) and Au@Ag core-shell NPs resulting from 3 (red), 5 (blue) and 10 (magenta) Ag^+ additions. The sizes of the Au NPs seeds were 15 nm (D), 32 nm (E) and 55 nm (F).

This strategy can be extended to other morphologies obtained using citrate as stabilizer. As an example, we used the same approach to coat citrate-stabilized gold nanostars synthesized by a surfactant free method.[42] As shown in Figure S6, SI, as the deposition of silver was increased, the particles tips become less apparent, suggesting a preferential Ag deposition on the central part of the Au nanostars. Additionally, Ag coating resulted in a strong blue shift of the main LSPR (Figure S6, SI), showing not only the deposition of a different metal but also a drastic change in the morphology of the NPs (decreasing the length and number of tips).

An obvious extension of this work is the study of the SERS properties of Au@Ag core-shell NPs. Although the SERS properties of gold and silver NPs of various morphologies have been extensively investigated,[43] the majority of the reported SERS studies have been performed on NPs immobilized on solid substrates. However, NPs dispersions exhibiting strong SERS signals are of great interest for many analytical and bio-imaging applications.[8,44,45] Interestingly, few studies have been reported focusing on the SERS properties of Ag colloids, mainly because of the existing limitations in size controlled synthesis.[46] It is well known that the SERS efficiency depends on the size of NPs as well as excitation wavelength due to the coupling between the excitation wavelength and LSPR of NPs.[44,46-48] Previous SERS studies were carried out on isolated particles or particles deposited on substrates and with different excitation laser lines, which makes it difficult to predict the particle size and excitation wavelength for maximum SERS efficiency.

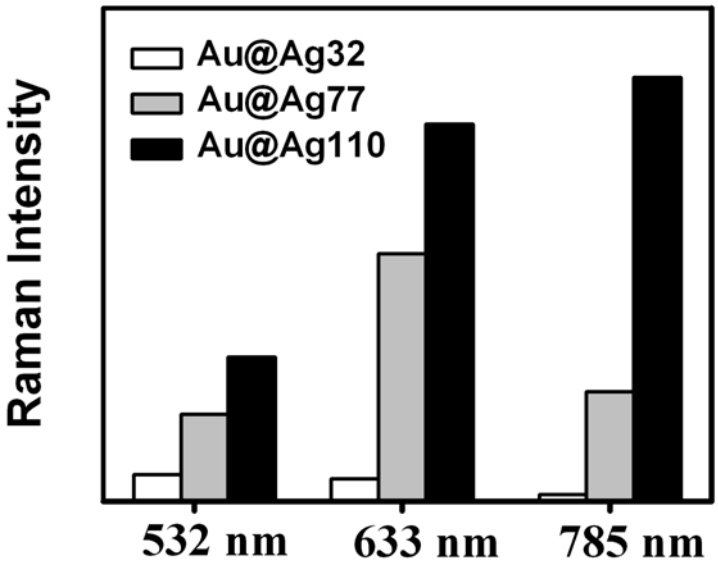

Figure 3. Comparison of the SERS intensity of the 1-NAT ring stretching peak (1368cm^{-1}) for the different Au@Ag core-shell NPs at three excitation wavelengths: 532, 633, and 785 nm**.** All spectra were recorded in solution.

First, the SERS properties of 32, 77, and 110 nm Au@Ag core-shell NPs dispersions were analyzed by using 1-NAT as Raman active probe, with three different excitation lasers ranging from the visible (532 and 633 nm) to the NIR (785) (Figure S7, SI). The SERS spectra show the characteristic SERS bands for 1-NAT: ring stretching (1553, 1503, and 1368 cm^{-1}), ring breathing (968 and 822 cm^{-1}), ring deformation (792, 664, 539, and 517 cm^{-1}), CH bending (1197 cm^{-1}), and CS stretching (389 cm^{-1}). The SERS intensity of the 1-NAT ring stretching peak (1368 cm^{-1}) for three different core@shell NPs with all excitation wavelengths is plotted in Figure 3. The results show that the SERS efficiency increased with the Au@Ag NP size regardless of the selected laser line (Figure 3). This might be due to the increase of near-E-field intensity with particle size (see E-field maps calculated at 532 nm irradiation for the different Au@Ag NPs in Figure S8, SI). It should be mentioned, the SERS intensity with respect to the excitation wavelength are not comparable as the power of the lasers are different. However, the intensity trends of the SERS intensity for three different size particles at three different lasers are different (Figure 3). As shown in Figure 3, the relative increase of SERS intensities with the increase of particle size is much higher at 785 nm excitation compared to 633, 532 nm excitations. This is because the SPR maximum for Au@Ag32 and Au@Ag77 NPs is quite far from the 785 nm excitation, which results the week coupling leading to weak SERS intensity. However, in the case of Au@Ag110 nm, the particles exhibit quite broad and red shifted extinction results strong electronic coupling of 785 nm laser with Au@Ag110 nm particles compared to Au@Ag32 and Au@Ag77. So Au@Ag110 nm NPS exhibit much higher SERS compared to other two sizes at 785nm excitation.

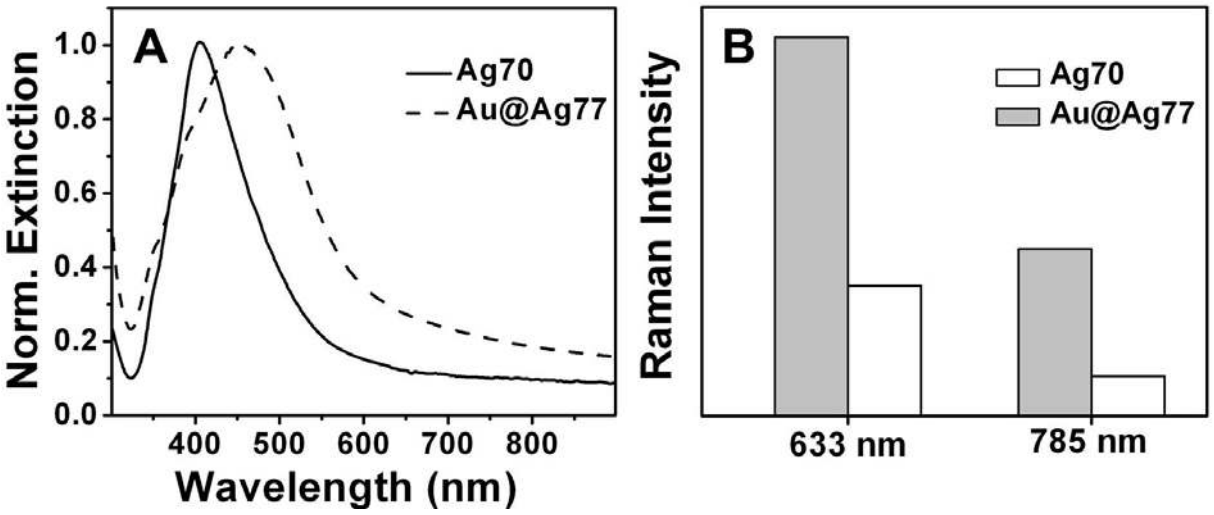

Figure 4. (A) Extinction spectra of Ag NPs of ~70 nm diameter prepared by citrate reduction (see TEM image in Figure S9, SI) and Au@Ag core-shell NPs ~77 nm outer diameter. (B) Comparison of the normalized SERS intensity of the 1-NAT ring stretching peak (1368 cm^{-1}) for ~77 nm Au@Ag NPs ~and ~70 nm Ag NPs , obtained upon excitation at 633 and 785 nm.

As both the experimental and theoretical extinction spectra of Au@Ag core-shell NPs are similar to those of pure Ag NPs (Figures S5, SI), we compared their SERS efficiency with that of conventional citrate reduced Ag NPs of nearly same size (Figure S9, SI). The normalized extinction spectra of 70 nm Ag NPs and 77 nm Au@Ag core-shell NPs are shown in Figure 4. Comparison of their SERS properties recorded using 633 and 785 nm laser lines shows that core-shell NPs consistently exhibit higher SERS efficiency (Figure 4). Nevertheless, nearly the same SERS efficiency was obtained with 532nm excitation (data not shown). The obtained results can be explained in terms of more effective coupling with the excitation laser for Au@Ag NPs because a higher extinction contribution of the core-shell NPs is observed above 600 nm (Figure 4A).

CONCLUSIONS

We have demonstrated a simple and efficient strategy for the size controlled synthesis of Au@Ag core-shell NPs capped with citrate (useful for many applications). The method is based on the stepwise reduction of Ag^+ ions on Au NPs by AA. The final size of the core-shell NP is tunable in a wide size range (demonstrated here from 30 to 110 nm) by simply changing the core size or by controlling the shell thickness (varying the number of reduction cycles). The optical properties of the synthesized core-shell NPs closely resemble those predicted by Mie theory for concentric spheres. More importantly, extinction spectra of the Au@Ag core-shell NPs are also in good agreement with numerically calculated extinction spectra of pure Ag NPs when Ag shell reaches a sufficient thickness, suggesting that such uniform Au@Ag core-shell NPs are a suitable alternative to polydisperse Ag NPs. In addition, SERS properties of Au@Ag core-shell NPs were investigated at three different excitation wavelengths and the SERS efficiency was found to increase with size, regardless of the laser line. Interestingly, such core-shell NPs exhibit higher SERS efficiency over conventional citrate capped Ag NPs at red or NIR excitation. Such core-shell NPs with superior SERS properties are thus expected to be excellent candidates for SERS based analytical and imaging applications.

Supporting Information: TEM images of the Au seeds, pure Ag and Au@Ag core-shell NPs. Measured extinction spectra of different Au@Ag core-shell colloids. Calculated spectra of different Ag colloids. Results obtained with Au nanostars. Calculated near-field maps for Au@Ag core-shell NPs. SERS spectra of 1-NAT on Au@Ag core-shell NPs. This material is available free of charge via the Internet at http://pubs.acs.org.

AUTHOR INFORMATION

Corresponding Author

*Phone (+34) 986813813 ; e-mail :pastoriza@uvigo.es (I.P.S)

Notes

The authors declare no competing interest

ACKNOWLEDGEMENTS

The authors wish to express their thanks to Dr. Amane Shiohara for the preparation of Au nanostars. This work has been also supported by the Spanish MINECO (grant MAT2010-15374 and CTQ 2010-18576) and by the Xunta de Galicia/FEDER (grant 10PXIB314218PR and INBIOMED, "unha maneira de facer Europa").

REFERENCES

(1) Polavarapu, L.; Liz-Marzán, L. M. Towards Low-cost Flexible Substrates for Nanoplasmonic Sensing. *Phys. Chem. Chem. Phys.* **2013**, *15*, 5288-5300.

(2) Anker, J. N.; Hall, W. P.; Lyandres, O.; Shah, N. C.; Zhao, J.; Van Duyne, R. P. Biosensing with Plasmonic Nanosensors. *Nat. Mater.* **2008**, *7*, 442-453.

(3) Jain, P. K.; Huang, X. H.; El-Sayed, I. H.; El-Sayed, M. A. Noble Metals on the Nanoscale: Optical and Photothermal Properties and Applications in Imaging, Sensing, Biology, and Medicine. *Acc. Chem. Res.* **2008**, *41*, 1578-1586.

(4) Polavarapu, L.; Venkatram, N.; Ji, W.; Xu, Q. H. Optical-limiting Properties of Oleylamine-capped Gold Nanoparticles for both Femtosecond and Nanosecond Laser Pulses. *ACS Appl. Mater. Interfaces* **2009**, *1*, 2298-2303.

(5) Dreaden E.C.; Alkilany A.M.; Huang X.; Murphy C.J.; El-Sayed M.A. The Golden Age: Gold Nanoparticles for Biomedicine. *Chem. Soc. Rev.* **2012**, 41, 2740-2779.

(6) Kreibig, U.; Vollmer, M. Optical Properties of Metal Clusters, Springer Series in Materials Science 25, New York, Springer-Verlag, **1995**.

(7) Liz-Marzán, L. M. Tailoring Surface Plasmon Resonance through the Morphology and Assembly of Metal Nanoparticles. *Langmuir* **2006**, *22*, 32-41.

(8) Cardinal, M. F.; Rodríguez-González, B.; Alvarez-Puebla, R. A.; Pérez-Juste, J.; Liz-Marzán, L. M. Modulation of Localized Surface Plasmons and SERS Response in Gold Dumbbells Through Silver Coating. *J. Phys. Chem. C* **2010**, *114*, 10417-10423.

(9) Jiang, R.; Chen, H.; Shao, L.; Li, Q.; Wang, J. Unraveling the Evolution and Nature of the Plasmons in (Au Core)−(Ag Shell) Nanorods. *Adv. Mater.* **2012**, *24*, OP200-OP207.

(10) Xie, F.; Baker, M. S.; Goldys, E. M. Homogeneous Silver-coated Nanoparticle Substrates for Enhanced Fluorescence Detection *J. Phys. Chem. B* **2006**, *110*, 23085-23091.

(11) Lee, Y. H.; Chen, H. J.; Xu, Q. H.; Wang, J. F. Refractive Index Sensitivities of Noble Metal Nanocrystals: The Effects of Multipolar Plasmon Resonances and the Metal Type. *J. Phys. Chem. C* **2011**, *115*, 7997-8004.

(12) Sondi, I.; Goia, D. V.; Matijevic, E. Preparation of Highly Concentrated Stable Dispersions of Uniform Silver Nanoparticles. *J. Colloid Interface Sci.* **2003**, *260*, 75-81.

(13) Sun, Y. G.; Xia, Y. N. Large-Scale Synthesis of Uniform Silver Nanowires Through a Soft, Self-Seeding, Polyol Process. *Adv. Mater.* **2002**, *14*, 833-837.

(14) Jin, R. C.; Cao, Y. W.; Mirkin, C. A.; Kelly, K. L.; Schatz, G. C.; Zheng, J. G. Photoinduced Conversion of Silver Nanospheres to Nanoprisms. *Science* **2001**, *294*, 1901-1903.

(15) Polavarapu, L.; Liz-Marzan, L. M. Growth and Galvanic Replacement of Silver Nanocubes in Organic Medium. *Nanoscale* **2013**, *5*, 4355-4361.

(16) Bastys, V.; Pastoriza-Santos, I.; Rodríguez-González, B.; Vaisnoras, R.; Liz-Marzán, L. M. Formation of Silver Nanoprisms with Surface Plasmons at Communication Wavelengths. *Adv. Funct. Mater.* **2006,** 16, 766-773.

(17) Zhang, Q.; Li, W.; Wen, L.-P.; Chen, J.; Xia, Y. Facile Synthesis of Ag Nanocubes of 30 to 70 nm in Edge Length with CF3COOAg as a Precursor. *Chem. Eur. J.* **2010**, *16*, 10234-10239.

(18) Wang, Y.; Wan, D.; Xie, S.; Xia, X.; Huang, C. Z.; Xia, Y. Synthesis of Silver Octahedra with Controlled Sizes and Optical Properties via Seed-mediated Growth. *ACS Nano* **2013**, *7*, 4586-4594.

(19) Evanoff, D. D.; Chumanov, Jr., G. Size-Controlled Synthesis of Nanoparticles. 1. "Silver-Only" Aqueous Suspensions via Hydrogen Reduction. *J. Phys. Chem. B* **2004**, *108*, 13948-13956.

(20) Panacek, A.; Kvitek, L.; Prucek, R.; Kolar, M.; Vecerova, R.; Pizurova, N.; Sharma, V. K.; Nevecna, T.; Zboril, R. Silver Colloid Nanoparticles: Synthesis, Characterization, and their Antibacterial Activity. *J. Phys. Chem. B* **2006**, *110*, 16248-16253.

(21) Lee, P. C.; Meisel, D. Adsorption and Surface-Enhanced Raman of Dyes on Silver and Gold Sols. *J. Phys. Chem.* **1982**, *86*, 3391-3395.

(22) Dong, X. Y.; Ji, X. H.; Wu, H. L.; Zhao, L. L.; Li, J.; Yang, W. S. Shape Control of Silver Nanoparticles by Stepwise Citrate Reduction. *J. Phys. Chem. C* **2009**, *113*, 6573-6576.

(23) Bastus, N. G.; Comenge, J.; Puntes, V. Kinetically Controlled Seeded Growth Synthesis of Citrate-Stabilized Gold Nanoparticles of up to 200 nm: Size Focusing versus Ostwald Ripening. *Langmuir* **2011**, *27*, 11098-11105.

(24) Kimling, J.; Maier, M.; Okenve, B.; Kotaidis, V.; Ballot, H.; Plech, A. Turkevich Method for Gold Nanoparticle Synthesis Revisited. *J. Phys. Chem. B* **2006**, *110*, 15700-15707.

(25) Liu, X.; Xu, H.; Xia, H.; Wang, D. Rapid Seeded Growth of Monodisperse, Quasi-Spherical, Citrate-Stabilized Gold Nanoparticles via H_2O_2 Reduction. *Langmuir* **2012**, *28*, 13720-13726.

(26) Ziegler C.; Eychmüller, A. Seeded Growth Synthesis of Uniform Gold Nanoparticles with Diameters of 15-300 nm. *J. Phys. Chem. C* **2011**, *115*, 4502–4506.

(27) Rodríguez-Fernández, J.; Pérez-Juste, J.; García de Abajo, F. J.; Liz-Marzán, L. M. Seeded Growth of Submicron Au Colloids with Quadrupole Plasmon Resonance Modes. *Langmuir* **2006**, *22*, 7007-7010.

(28) Zhang, X.; Wang, H.; Su, Z. Fabrication of Au@Ag Core−Shell Nanoparticles Using Polyelectrolyte Multilayers as Nanoreactors. *Langmuir* **2012**, *28*, 15705-15712.

(29) Bohren, C. F.; Huffman, D. R. *Absorption and Scattering of Light by Small Particles*; John Wiley & Sons: New York, **1998.**

(30) Sánchez-Iglesias, A.; Carbó-Argibay, E.; Glaria, A.; Rodríguez-González, B.; Pérez-Juste, J.; Pastoriza-Santos, I.; Liz-Marzán, L. M. Rapid Epitaxial Growth of Ag on Au Nanoparticles: From Au Nanorods to Core-shell Au@Ag Octahedrons. *Chem. Eur. J.* **2010**, *16*, 5558-5563.

(31) Lim, D.-K.; Kim, I.-J.; Nam, J.-M. DNA-Embedded Au/Ag Core-Shell Nanoparticles. *Chem. Commun.* **2008**, 5312-5314.

(32) Gong, J.; Zhou, F.; Li, Z.; Tang, Z. Synthesis of Au@Ag Core−Shell Nanocubes Containing Varying Shaped Cores and their Localized Surface Plasmon Resonances. *Langmuir* **2012**, *28*, 8959−8964.

(33) Rodríguez-González, B.; Burrows, A.; Watanabe, M.; Kiely, C. J.; Liz-Marzán, L. M. Multishell Bimetallic AuAg Nanoparticles: Synthesis, Structure and Optical Properties. *J. Mater. Chem.* **2005**, *15*, 1755-1759.

(34) Liu, B.; Han, G.; Zhang, Z.; Liu, R.; Jiang, C.; Wang, S.; Han, M.-Y. Shell Thickness-Dependent Raman Enhancement for Rapid Identification and Detection of Pesticide Residues at Fruit Peels. *Anal. Chem*. **2012**, *84*, 255−261.

(35) Freeman, R. G.; Hommer, M. B.; Grabar, K. C.; Jackson, M. A.; Natan, M. J. Ag-Clad Au Nanoparticles: Novel Aggregation, Optical, and Surface-Enhanced Raman Scattering Properties. *J. Phys. Chem.* **1996**, *100*, 718-724.

(36) Turkevich, J.; Stevenson, P.C.; Hillier J. A Study of the Nucleation and Growth Processes in the Synthesis of Colloidal Gold. *Discuss. Faraday Soc.*, **1951**, *11*, 55-75.

(37) García de Abajo, F. J.; Howie, A. Relativistic Electron Energy Loss and Electron-Induced Photon Emission in Inhomogeneous Dielectrics. *Phys. Rev. Lett.* **1998**, *80*, 5180-5183.

(38) García de Abajo, F. J.; Howie, A. Retarded Field Calculation of Electron Energy Loss in Inhomogeneous Dielectrics. *Phys. Rev. B* **2002**, *65*, 115418-1-17.

(39) Johnson, P. B.; Christy, R. W. Optical Constants of the Noble Metals. *Phys. Rev. B* 1972, *6*, 4370-4379.

(40) Rodríguez-Lorenzo, L.; de la Rica, R.; Alvarez-Puebla, R. A.; Liz-Marzán, L. M.; Stevens, M. M. Plasmonic Nanosensors with Inverse Sensitivity by Means of Enzyme-Guided Crystal Growth. *Nat. Mater,* 2012, *11*, 604-607.

(41) Jana, N. R.; Gearheart, L.; Murphy, C. J. Seeding Growth for Size Control of 5−40 nm Diameter Gold Nanoparticles. *Langmuir*, **2001**, *17*, 6782-6786.

(42) Yuan, H. K.; Khoury, C. G.; Hwang, H.; Wilson, C. M.; Grant, G. A.; Vo-Dinh, T. Gold Nanostars: Surfactant-free Synthesis, 3D Modelling, and Two-Photon Photoluminescence Imaging. *Nanotechnology* **2012**, *23*, 075102

(43) Fan, M. K.; Andrade, G. F. S.; Brolo, A. G. A Review on the Fabrication of Substrates for Surface Enhanced Raman Spectroscopy and their Applications in Analytical Chemistry. *Anal. Chim. Acta* 2011, *693*, 7-25.

(44) Njoki, P. N.; Lim, I. I. S.; Mott, D.; Park, H.-Y.; Khan, B.; Mishra, S.; Sujakumar, R.; Luo, J.; Zhong, C.-J. Size Correlation of Optical and Spectroscopic Properties for Gold Nanoparticles. *J. Phys. Chem. C* 2007, *111*, 14664-14669.

(45) Pierre, M. C. S.; Mackie, P. M.; Roca, M.; Haes, A. J. Correlating Molecular Surface Coverage and Solution-Phase Nanoparticle Concentration to Surface-Enhanced Raman Scattering Intensities*J. Phys. Chem. C* **2011**, *115*, 18511-18517.

(46) Seney, C. S.; Gutzman, B. M.; Goddard, R. H. Correlation of Size and Surface-Enhanced Raman Scattering Activity of Optical and Spectroscopic Properties for Silver Nanoparticles *J. Phys. Chem. C* **2009**, *113*, 74-80.

(47) Ye, J.; Hutchison, J. A.; Uji-i, H.; Hofkens, J.; Lagae, L.; Maes, G.; Borghs, G.; Van Dorpe, P. Excitation Wavelength Dependent Surface Enhanced Raman Scattering of 4-aminothiophenol on Gold Nanorings. *Nanoscale* **2012**, *4*, 1606-1611.

(48) McFarland, A. D.; Young, M. A.; Dieringer, J. A.; Van Duyne, R. P. Wavelength-Scanned Surface-Enhanced Raman Excitation Spectroscopy. *J. Phys. Chem. B* **2005**, *109*, 11279-11285.

TOC Figure

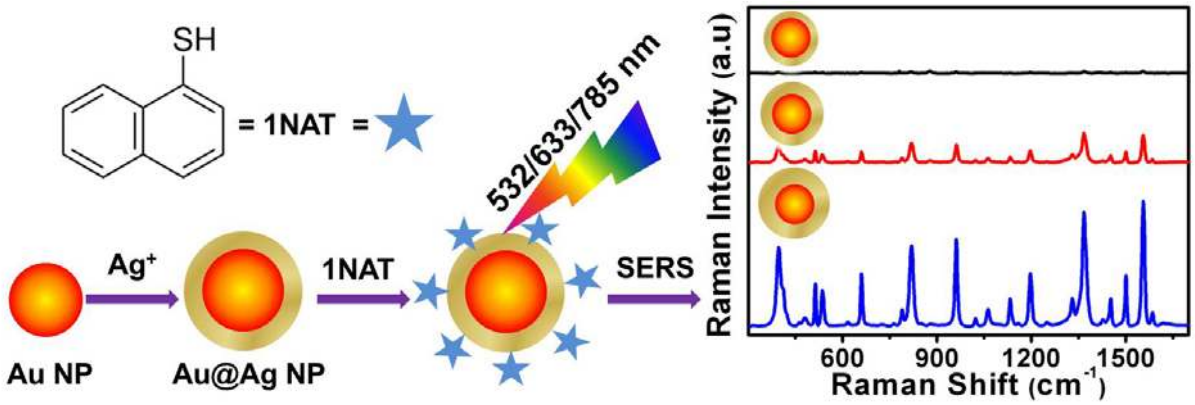
SH
= 1NAT =
532/633/785 nm
Ag+
1NAT
SERS
Au NP
Au@Ag NP
Raman Intensity (a.u)
600
900
1200
1500
Raman Shift (cm-1)